Electronic Supplementary Material (ESI) for Journal of Materials Chemistry A.
This journal is © The Royal Society of Chemistry 2022

Electronic Supplementary Information (ESI)

Mesh-like BiOBr/Bi_2S_3 nanoarray heterojunction with hierarchical pores and oxygen vacancies for broadband CO_2 photoreduction

Yamin Xi,[a] Weihao Mo,[a] Zhixin Fan,[a] Lingxuan Hu,[a] Wenbin Chen,[a] Yan Zhang,[a] Peng Wang,[b] Shuxian Zhong,[b] Yuling Zhao,[a] Song Bai*[a]

[a] Key Laboratory of the Ministry of Education for Advanced Catalysis Materials, College of Chemistry and Life Sciences, Zhejiang Normal University, Jinhua, Zhejiang 321004, P. R. China.

[b] College of Geography and Environmental Sciences, Zhejiang Normal University, Jinhua, Zhejiang, 321004, P. R. China

E-mail: songbai@zjnu.edu.cn

Experimental section

Materials

All chemicals were of analytical grade and purchased from Sinopharm Chemical Reagent Co. Ltd. (Shanghai, China), which were used as received without further purification. The water used in all experiments was de-ionized water prepared by passing through an ultra-pure purification system.

Synthesis of BiOBr nanoplates

In a typical synthesis of BiOBr-010 nanoplates, 1 mmol of $Bi(NO_3)_3{\cdot}5H_2O$ and 1 mmol of KBr were added to 15 mL water, and stirred continuously for 30 min. Then 15 mL of KBr solution was slowly dropped into the $Bi(NO_3)_3$ solution and the pH value was adjusted to 6.0 with 1 M NaOH aqueous solution. The mixture solution was poured into a 50 mL Teflon-lined stainless autoclave and heated at 220 ^{o}C for 24 h. After naturally cooling down to room temperature, the precipitates were separated by centrifuging at 5000 rpm for 10 min, washed with ethanol and water thoroughly, and dried at 60 ^{o}C in a vacuum. For comparison, BiOBr-001 nanoplates were prepared by following the same preparation process as BiOBr-010, except for adjusting the pH value of the reaction solution to 1.0 with 1 M NaOH aqueous solution.[S1]

Synthesis of BiOBr/Bi_2S_3 heterojunctions

In a typical synthesis of BiOBr/Bi_2S_3 heterojunctions with optimal Bi_2S_3 loading amount of 34%, 20 mL of H_2O was injected into a 50 mL round bottom flask, and the pH of which was adjusted to 2.5 by 0.5 M HCl. Subsequently, thioacetamide (TAA, 30 mg, 0.4 mmol) was added into the solution and stirred for 10 min, followed by the addition of 120 mg of BiOBr precursor. The resulting mixture was sonicated for 5 min and heated at 80 ^{o}C for 2 h in an oil bath. After naturally cooling down to room temperature, the product was collected by centrifuging, washed with ethanol and water thoroughly, and dried at 45 °C in a vacuum. In order to monitor the structural evolution of the heterojunctions, intermediate products were collected at reaction times of 0.5, 1.0 and 1.5 h, respectively. As for the synthesis of BiOBr/Bi_2S_3 with Bi_2S_3 loading amounts of 7%, 20% and 50%, 400, 240 and 30 mg of BiOBr-010 nanoplates were used, respectively.

Synthesis of pure Bi_2S_3

Pre-synthesized BiOBr-010 nanoplates (60 mg, 0.2 mmol) were dispersed in 10 mL water and magnetically stirred for 20 min. Afterwards, 10 mL of TAA (30 mg, 0.4 mmol) aqueous solution was added into the suspension, followed by magnetically stirring for 20 min. The mixture was transferred to a 50 mL Teflon-lined stainless steel autoclave and heated at 180 °C for 2 h. After cooling down to ambient temperature naturally, the resulting precipitates were collected and washed with water and ethanol for several times to remove the residual impurities, and finally dried at 45 °C in a vacuum. To monitor the structural evolution of BiOBr-001 nanoplates during the TAA treatment, the same experimental process was carried out for 3, 6 and 9 h except the use of the same amount of BiOBr-001 instead of BiOBr-010 as precursor.

Photocatalytic CO_2 reduction measurements

To investigate the photocatalytic performance of the samples in CO_2 reduction, 30 mg of photocatalysts was dispersed in 8 mL of a water/triethanolamine mixture (8 mL, 1:1, v:v). The mixture was sonicated to form a uniform suspension in a 100 mL reactor (Beijing Perfectlight, China), followed by purging the reactor with CO_2 to eliminate air. Then the light-irradiation experiment was performed by using a 300 W Xe lamp (PLS-SXE300D/300DUV, Beijing Perfectlight, China). The power density of light was measured to be 100 mW cm^{-2} for full spectrum ($\lambda > 320$ nm) using a radiometer (FZ-A, China). The photocatalytic reaction was conducted for 4 h with stirring at 600 rpm. The gaseous mixture was analyzed using a gas chromatograph (GC-2014, Shimadzu) with Ar as the carrier gas. The CO was converted to CH_4 via a methanation reactor and then analyzed using a thermal conductivity detector (FID). The produced H_2 was analyzed through a TCD.

During the stability test, the photocatalyst was collected after each run and then reused for the photocatalytic reaction. The wavelength-dependent photocatalytic performance was measured using the Xe lamp equipped with 365, 400, 450, 500, 550, 600, 650, 700, 750 and 800 nm band-pass filters, respectively.

$$\text{CO selectivity (\%)} = [2v(\text{CO})]/[2v(\text{H}_2) + 2v(\text{CO})] \times 100\% \qquad (1)$$

where $v(\text{CO})$ and $v(\text{H}_2)$ stand for the formation rates of CO and H_2.

The rate constant of CO (k_{CO}) was calculated according to the method reported in previous literature.[S2] Generally, the photocatalytic CO_2 reduction process can be described by a series of independent first-order model, namely:

$$\frac{d[\text{CO}_2]}{dt} = -k_1[\text{CO}_2] \qquad (2)$$

$$\frac{d[\text{CO}]}{dt} = k_1[\text{CO}_2] - k_2[\text{CO}] \qquad (3)$$

where t is reaction time, k_1 and k_2 are the reaction rate constants of CO_2 and CO, respectively. Since Equation 2 and 3 are sequential, they can be resolved using the following initial condition, $[\text{CO}]_0 = 0$.

$$[\text{CO}_2] = [\text{CO}_2]_0 e^{-k_1 t} \qquad (4)$$

$$[\text{CO}] = \frac{k_1[\text{CO}_2]_0}{k_2 - k_1}(e^{-k_1 t} - e^{-k_2 t}) \qquad (5)$$

Electrochemical and photoelectrochemical measurements

5.0 mg of as-prepared samples was uniformly mixed with 15 μL of Nafion and 15 μL of ethanol, which were then uniformly coated onto a 1 cm × 1 cm indium tin oxide (ITO) glass. Subsequently, the coated ITO glass was dried at 50 °C for 3 h in vacuum. The electrochemical measurements were performed on a CHI 760E electrochemical station (Shanghai Chenhua, China). A standard three electrode system was used consisting of the ITO glass as work electrode, an Ag/AgCl electrode as reference electrode, and a Pt foil as counter electrode, which were inserted in a quartz cell containing 0.5 M Ar-saturated Na_2SO_4 electrolyte. Electrochemical impedance spectroscopy (EIS) was performed in the 10^1 to 10^5 Hz frequency range with an AC voltage amplitude of 10 mV at an applied potential of 0.2 V vs. Ag/AgCl. For the Mott-Schottky experiment, the potential were ranged from -2.0 to 1.0 V (vs. Ag/AgCl), and the frequency were 0.5, 0.75, and 1.0 kHz, respectively. The photoelectrochemical tests were performed in ambient conditions under irradiation of a 300 W Xe lamp (PLS-SXE300D/300DUV, Beijing Perfectlight, China). The power density of the light was measured to be 100 mW cm^{-2} for full spectrum. The photocurrent density vs. time (I-t) curves of the prepared photoelectrodes was operated at an applied potential of 0.2 V vs. Ag/AgCl under chopped light irradiation (light on/off cycles: 60 s) for 600 s. The transient open-circuit voltage decay (OCVD) measurements were taken for a total of 800 s, and the light was switched on and off after 100 and 400 s from the start, respectively. The average lifetimes of the photogenerated carriers (τ_n) was then estimated from the open-circuit voltage (V_{oc}) decay according to the following Equation:

$$\tau_n = -\frac{k_B T}{q}\left(\frac{dV_{oc}}{dt}\right)^{-1} \tag{6}$$

where τ_n represents the average lifetime, V_{oc} is open-circuit voltage, k_B is the Boltzmann constant, T is the temperature (in Kelvin), and q is the unsigned charge of an electron.

Sample characterizations

Transmission electron microscopy (TEM), high-resolution TEM (HRTEM), selected-area electron diffraction (SAED), scanning TEM (STEM) and energy dispersive spectroscopy (EDS) mapping profiles were taken on a JEOL JEM-2100F field-emission high-resolution transmission electron microscope operated at 200 kV. Scanning electron microscopy (SEM) characterization was carried out on a Zeiss Gemini 300 scanning electron micro-analyzer with an accelerating voltage of 5 kV. Powder X-ray powder diffraction (XRD) patterns were collected on a D8 Advance X-ray diffractometer with Non-monochromated Cu-Kα X-Ray. X-ray photoelectron spectra (XPS) were collected on an ESCALab 250 X-ray photoelectron spectrometer, using nonmonochromatized Al-Kα X-ray as the excitation source. Brunauer-

Emmett-Teller (BET) specific surface areas and N_2 adsorption were measured by using a Quantachrome autosorb iQ analyzer at 77 K. CO_2 adsorption was tested using the Quantachrome autosorb iQ analyzer at 298 K. Stead-state photoluminescence (PL) emission spectrum was recorded by a photoluminescence spectrometer (FLS980, Edinburgh) with a 375 nm excitation wavelength. The electron spin resonance (ESR) signal was examined by Bruker EMXplus EPR spectrometer. CO_2 temperature-programmed desorption (CO_2-TPD) was performed on a Micromeritics AutoChem II 2920 chemisorption equipment with a thermal conductivity detector (TCD). The samples were heated to 400 ^{o}C for 1 h with He as the carrier gas (30 mL min^{-1}). When the temperature dropped below 50 °C, 10% CO_2/He mixture (30 mL min^{-1}) was evacuated for 30 min. Then desorption was carried out with He as the carrier gas (30 mL min^{-1}) at a heating rate of 30 ^{o}C min^{-1} in the temperature range of 50-800 ^{o}C. In situ diffuse reflectance Fourier transform infrared spectroscopy (DRIFTS) was conducted with an in-situ diffuse reflectance Fourier transform infrared spectrometer (Nicolet iN10). UV-vis diffuse reflectance data were recorded in the spectral region of 200-1600 nm with a Cary-7000 series UV-vis-NIR spectrophotometer. The Tauc plot was deduced from the UV-vis diffuse reflectance according to the equation:

$$(\alpha h\nu)^n = A(h\nu - E_g) \tag{7}$$

where α is the absorption coefficient, $h\nu$ is the light energy, E_g is the optical bandgap, and n is equal to 1/2 for indirect bandgap BiOBr and Bi_2S_3.

Theoretical simulations

The present first principle DFT calculations were performed by Vienna Ab initio Simulation Package (VASP) with the projector augmented wave (PAW) method.[S3,4] The exchange-functional was treated using the generalized gradient approximation (GGA) of Perdew-Burke-Ernzerhof (PBE) functional.[S5] The energy cutoff for the plane wave basis expansion was set to 400 eV and the force on each atom less than 0.03 eV/Å was set for convergence criterion of geometry relaxation. A 15 Å vacuum was added along the z direction in order to avoid the interaction between periodic structures. The Brillouin zone integration was performed using 5×1×1 k-point sampling. The self-consistent calculations applied a convergence energy threshold of 10^{-5} eV. The DFT-D3 method was employed to consider the van der Waals interaction.[S6] In this work, CO_2 reduction was considered as followed:

$$* + CO_2 + H^+ + e^- \rightarrow *COOH \tag{8}$$

$$*COOH + H^+ + e^- \rightarrow *CO \tag{9}$$

$$*CO \rightarrow * + CO \tag{10}$$

Here, the asterisk (*) represents the surface substrate active site. The free energies of the CO_2 reduction steps (CRR) were calculated by the equation:[S7] $\Delta G = \Delta E_{DFT} + \Delta E_{ZPE} - T\Delta S$, where ΔE_{DFT} is the DFT electronic energy difference of each step, ΔE_{ZPE} and ΔS are the correction of zero-point energy and the variation of entropy, respectively, which are obtained by vibration analysis, T is the temperature (T = 300 K).

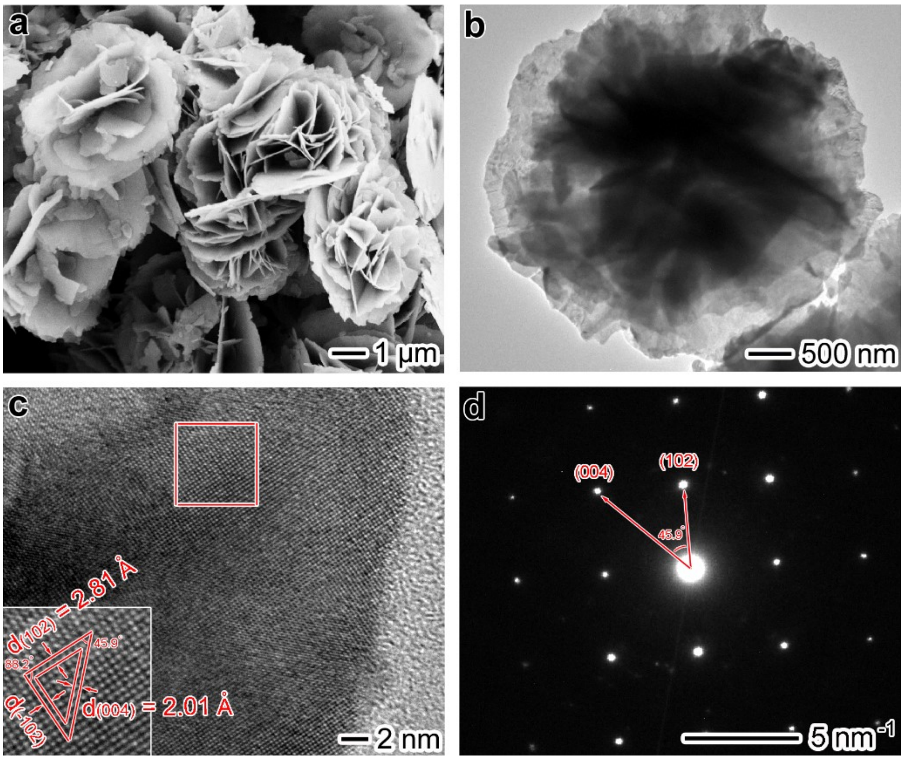

Fig. S1 (a) SEM, (b) TEM, (c) HRTEM images and (d) SAED pattern of BiOBr-010 nanoplates.

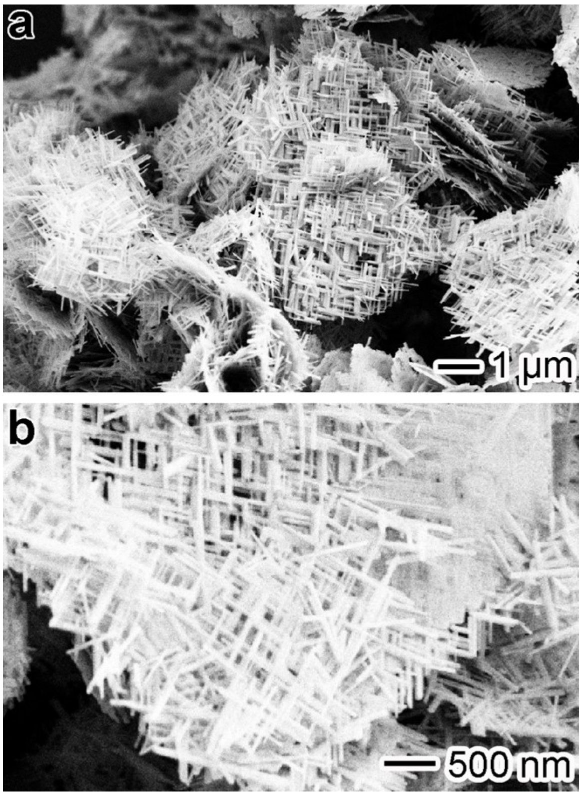

Fig. S2 TEM images of bare Bi_2S_3 obtained by the complete sulfurization of BiOBr-010 nanoplates with TAA through a hydrothermal reaction at 180 ^{o}C.

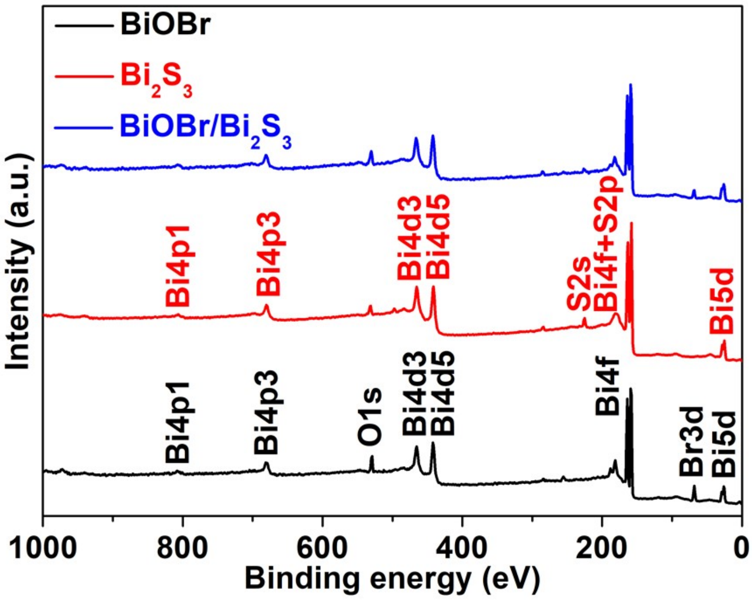

Fig. S3 Survey XPS spectrum of BiOBr, Bi_2S_3 and BiOBr/Bi_2S_3.

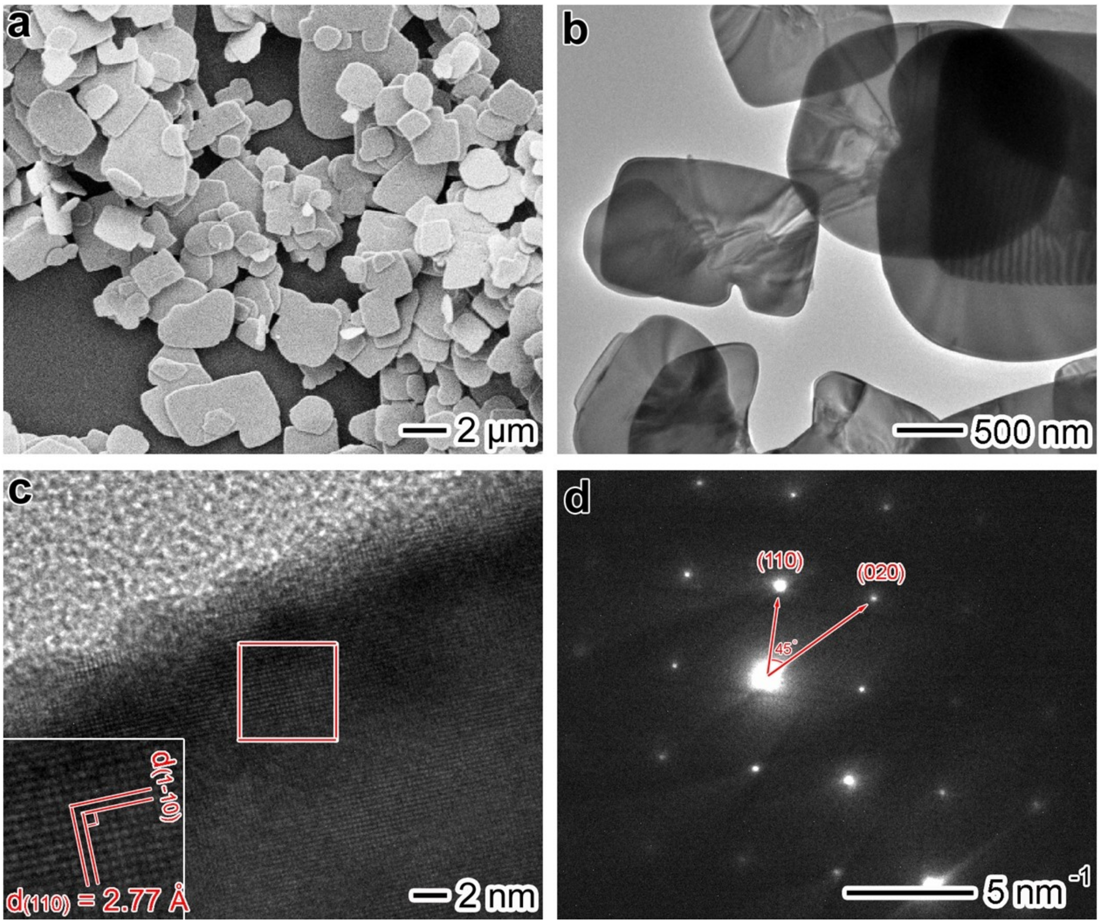

Fig. S4 (a) SEM, (b) TEM, (c) HRTEM images and (d) SAED pattern of BiOBr-001 nanoplates.

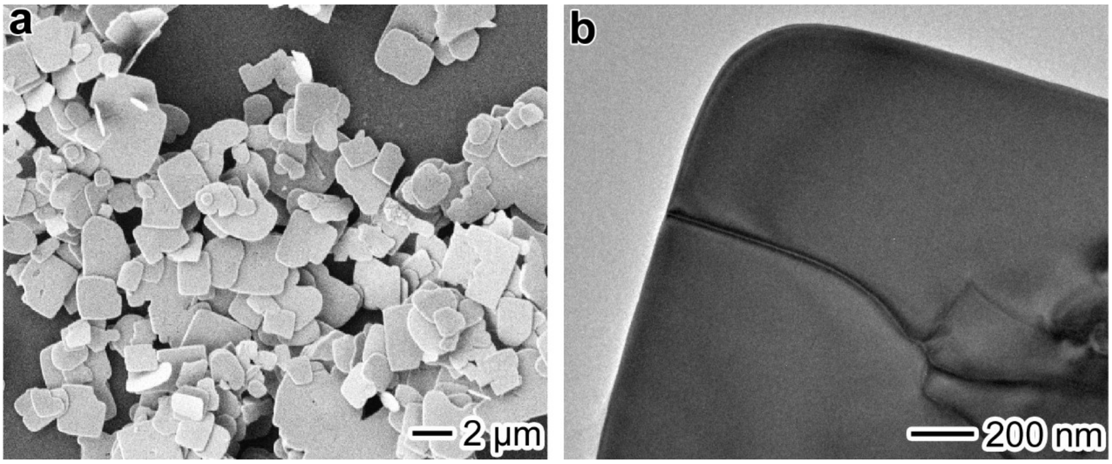

Fig. S5 (a) SEM and (b) TEM images of BiOBr-001 nanoplates after the TAA treatment (oil bath, 80 ^{o}C) following the same synthetic procedure of BiOBr/Bi_2S_3 heterojunction.

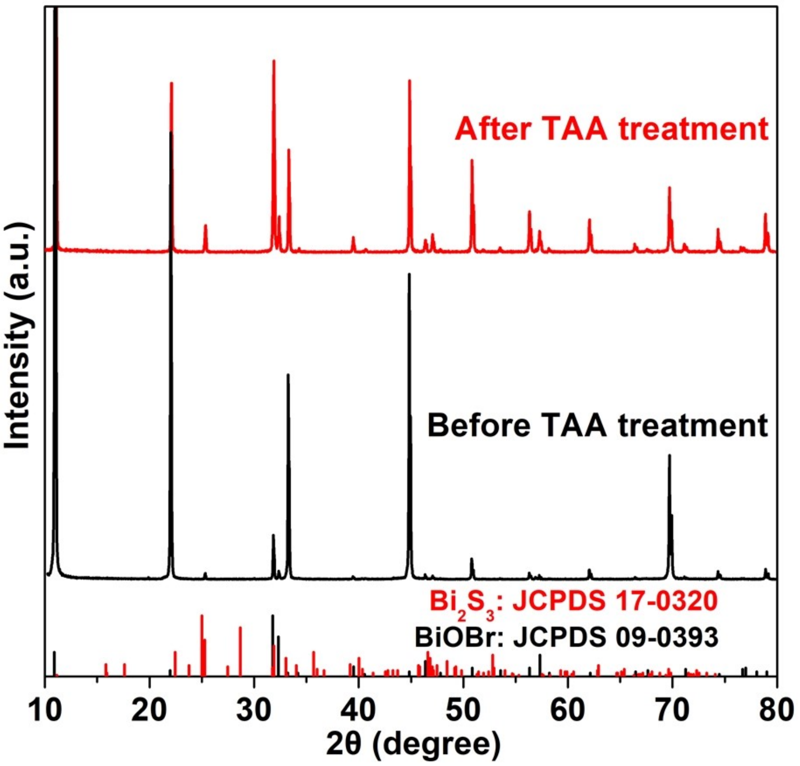

Fig. S6 XRD patterns of BiOBr-001 nanoplates before and after TAA treatment (oil bath, 80 °C) following the same synthetic procedure of BiOBr/Bi_2S_3 heterojunction.

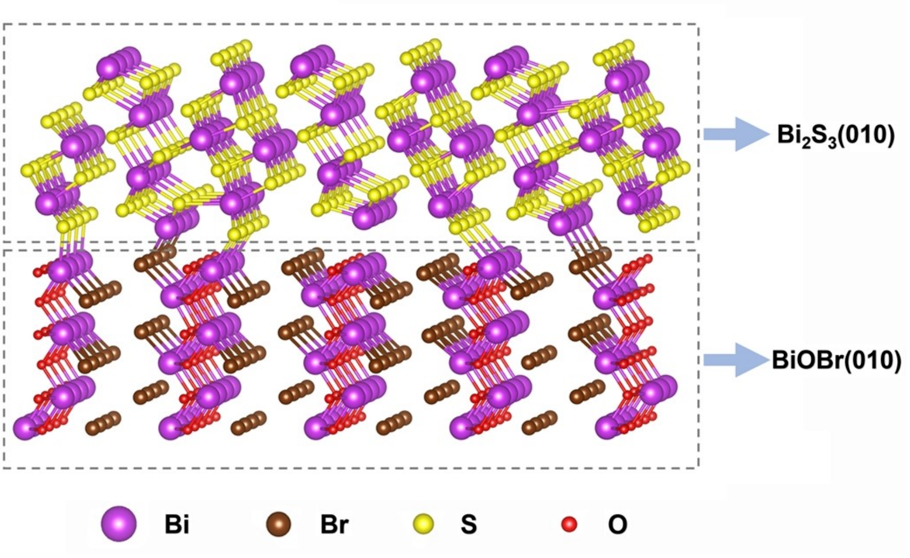

Fig. S7 Calculated model of BiOBr(010)-Bi_2S_3(010) interface

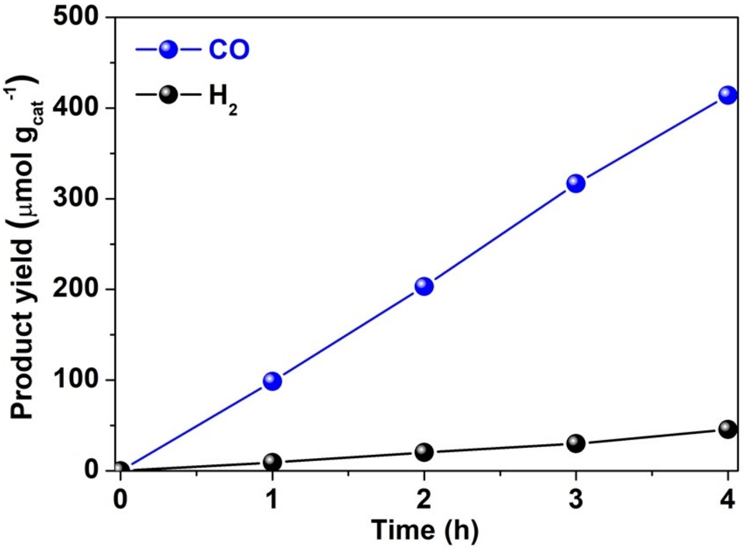

Fig. S8 Yields of CO and H_2 over BiOBr/Bi_2S_3-34 in 4 h under broadband light irradiation.

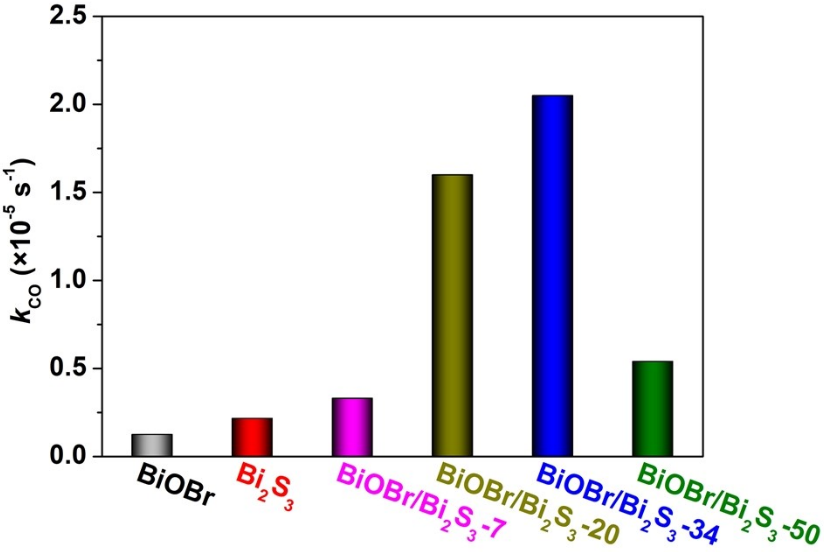

Fig. S9 Rate constants of CO_2 reduction to CO over different samples.

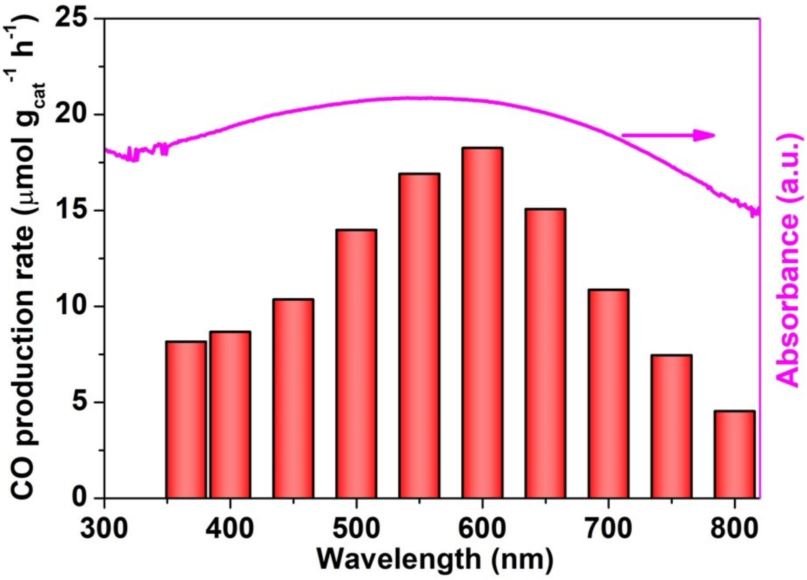

Fig. S10 Wavelength-dependent CO production rates of BiOBr/Bi_2S_3-34.

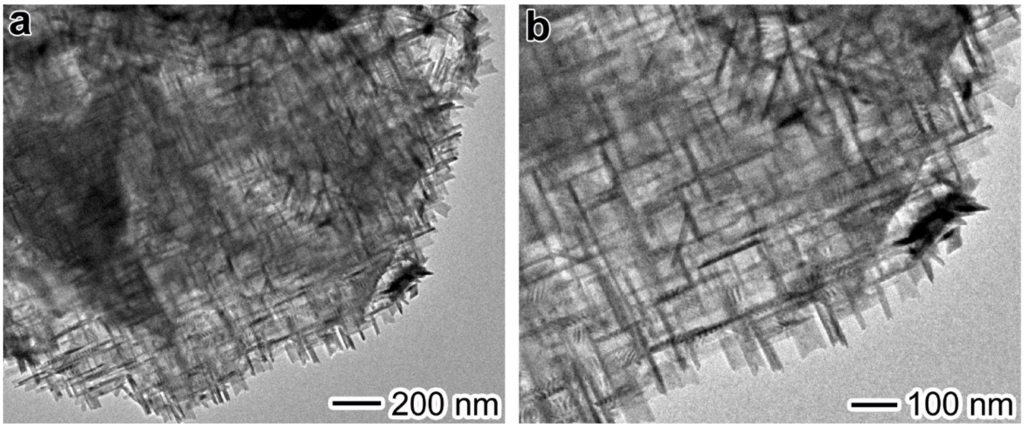

Fig. S11 TEM images of BiOBr/Bi_2S_3-34 after the photocatalytic reaction.

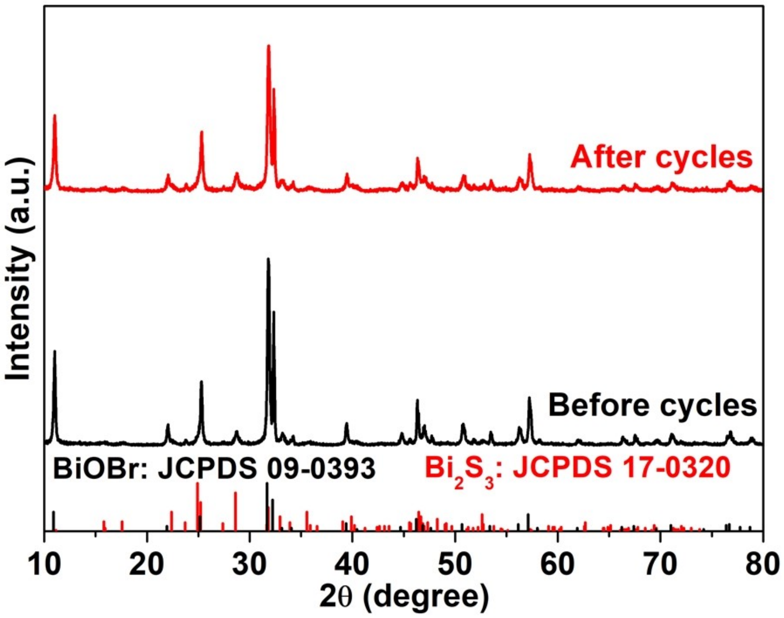

Fig. S12 Comparative XRD patterns of BiOBr/Bi_2S_3-34 before and after the photocatalytic reaction.

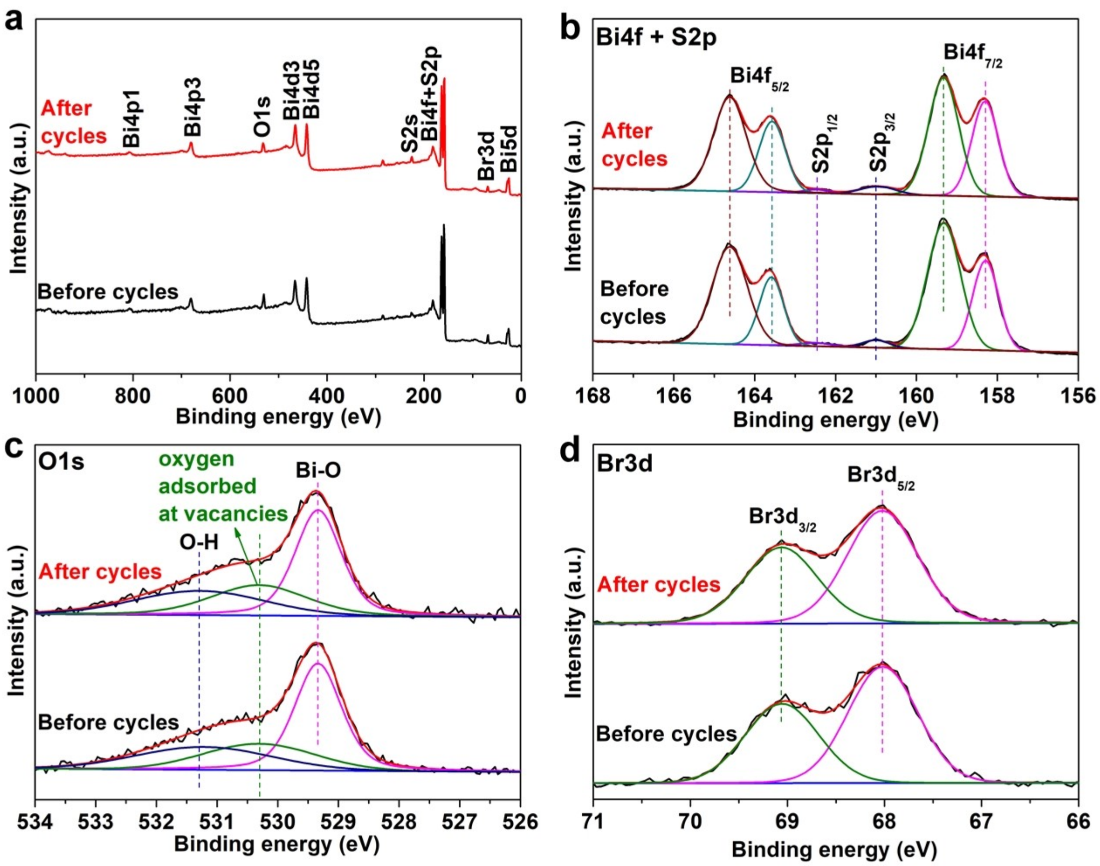

Fig. S13 Comparative XPS spectra of BiOBr/Bi_2S_3-34 before and after the photocatalytic reaction: (a) survey spectra, (b) Bi4f + S2p, (c) O1s, and (d) Br3d.

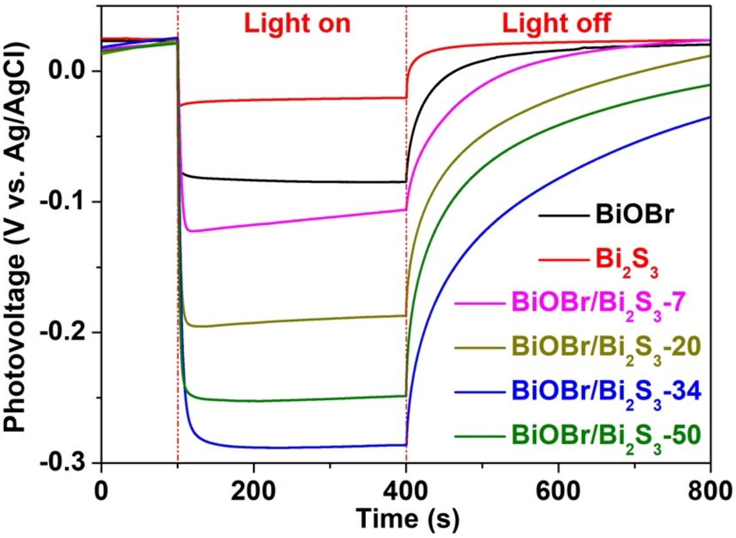

Fig. S14 Photovoltage transient rise/decay of as-prepared samples obtained during startup/termination of broadband light irradiation.

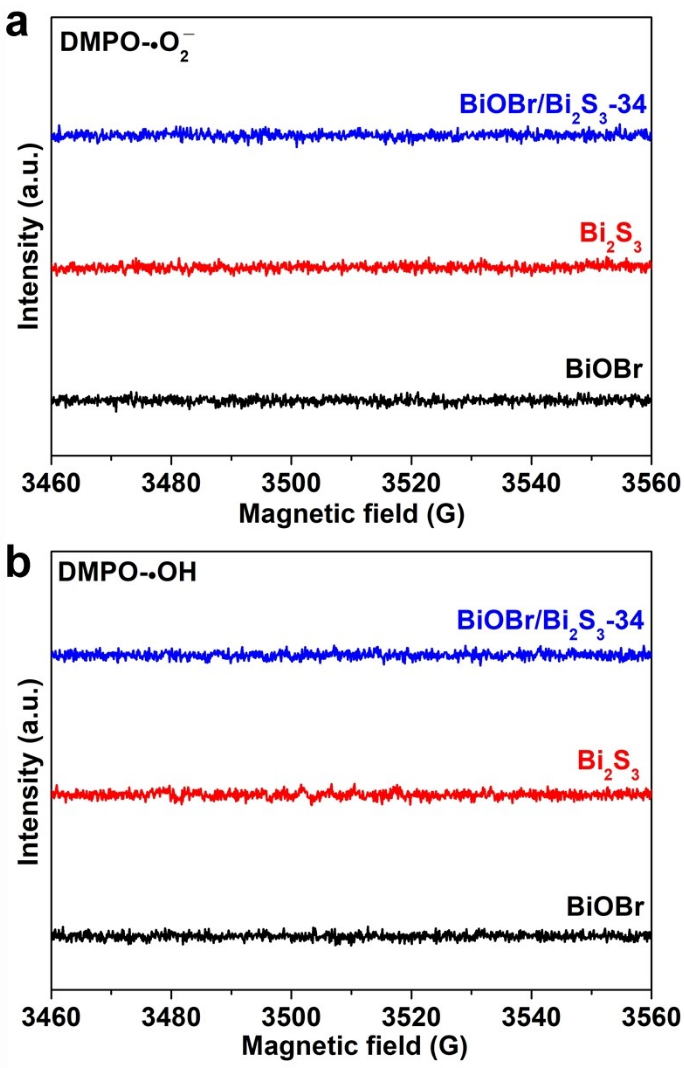

Fig. S15 Spin-trapping ESR spectra of (a) DMPO-$\bullet O_2^-$ and (b) DMPO-•OH over BiOBr, Bi_2S_3 and BiOBr/Bi_2S_3-34 in the dark.

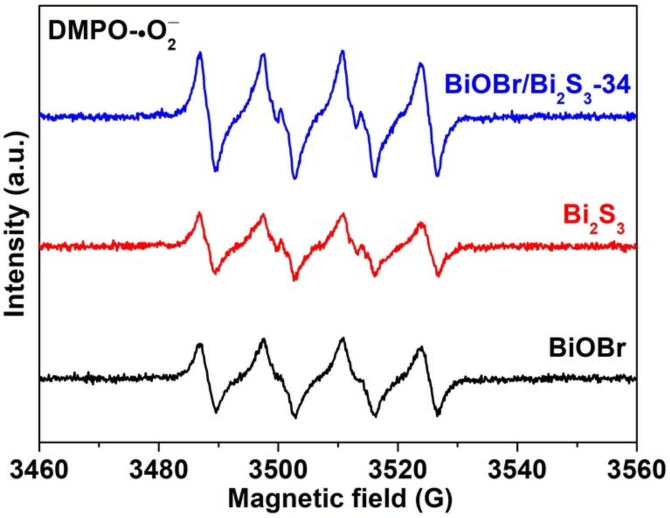

Fig. S16 Spin-trapping ESR spectra of DMPO-•O_2^- over BiOBr, Bi_2S_3 and BiOBr/Bi_2S_3-34 under broadband light irradiation.

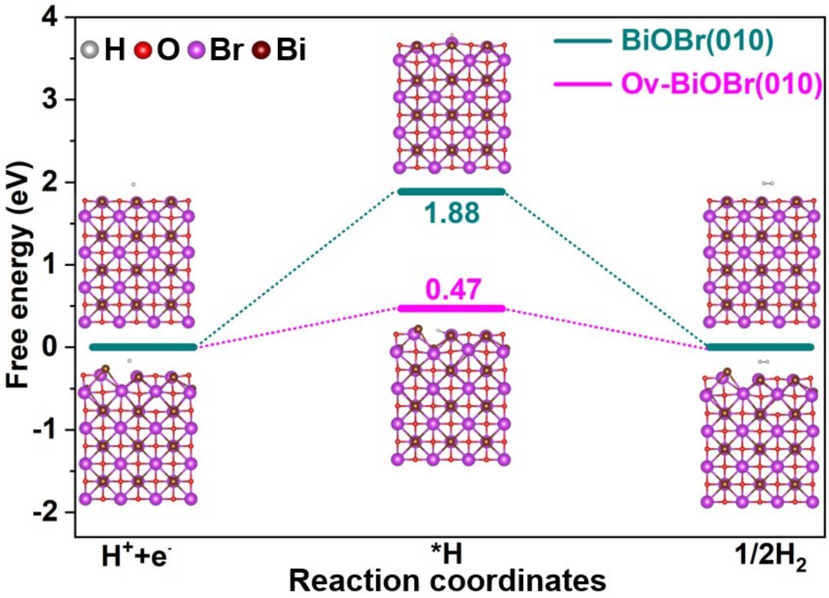

Fig. S17 Free energy diagrams of H_2 evolution on BiOBr(010) and V_O-BiOBr(010).

Table S1. Comparison of the photocatalytic performance of optimized BiOBr/Bi_2S_3 nanoarray heterojunction in CO_2 reduction with those of previously reported BiOBr/Bi_2S_3 heterojunction and BiOBr-based photocatalysts.

Photocatalyst	**Light source**	**CO production rate (μmol g_{cat}^{-1} h^{-1})**	**Reference**
BiOBr/Bi_2S_3-34	300 W Xe lamp 100 mW cm^{-2} $\lambda > 320$ nm	103.5	This work
BiOBr/Bi_2S_3 microspheres	300 W Xe lamp	100.8	S8
BiOBr hollow spheres	300 W Xe lamp	88.10	S9
V_O-BiOBr atomic layers	300 W Xe lamp $\lambda > 400$ nm	87.40	S10
BiOBr/Co_2N	300 W Xe lamp 150 mW cm^{-2}	67.80	S11
V_O-BiOBr/C_3N_4	300 W Xe lamp	61.80	S12
V_O-BiOBr/HNb_3O_8	300 W Xe lamp	32.92	S13
V_{BiO}-BiOBr	300 W Xe lamp	24.97	S14
BiOBr/cardon spheres	300 W Xe lamp	23.74	S15
BiOBr-nanoplates	300 W Xe lamp 200 mW cm^{-2}	21.60	S16
V_{Bi}-BiOBr	300 W Xe lamp	20.10	S17
$BiOBr_{0.6}Cl_{0.4}$	300 W Xe lamp 200 mW cm^{-2}	15.86	S18
BiOBr/$Bi_{24}O_{31}Br_{10}$	300 W Xe lamp	5.84	S19
BiOBr-001 nanoplates	300 W Xe lamp 210 mW cm^{-2}	4.45	S20
Hollow $Bi_4O_5Br_2$	300 W Xe lamp	3.16	S21
BiOBr/$BiPO_4$/Bi	300 W Xe lamp $\lambda \geq 400$ nm	3.14	S22
$Bi_4O_5Br_2$	300 W Xe lamp $\lambda \geq 400$ nm	2.73	S23
Ultrathin BiOBr	300 W Xe lamp $\lambda \geq 400$ nm	2.67	S23
BiOBr/Bi_2O_4	300 W Xe lamp	2.60	S24
V_O-BiOBr	300 W Xe lamp $\lambda \geq 400$ nm	2.03	S25

References

S1 M. Shi, G. N. Li, J. M. Li, X. Jin, X. P. Tao, B. Zeng, E. A. Pidko, R. G. Li and C. Li, *Angew. Chem., Int. Ed.*, 2020, **59**, 6590-6595.

S2 Y. P. Peng, Y. T. Yeh, S. I. Shah and C. P. Huang, *Appl. Catal. B: Environ.*, 2012, **123-124**, 414-423.

S3 G. Kresse and J. Furthmüller, *Comp. Mater. Sci.*, 1996, **6**, 15-50.

S4 P. E. Blöchl, *Phys. Rev. B*, 1994, **50**, 17953.

S5 J. P. Perdew, J. A. Chevary, S. H. Vosko, K. A. Jackson, M. R. Pederson, D. J. Singh and C. Fiolhais, *Phys. Rev. B*, 1992, **46**, 6671.

S6 S. Grimme, J. Antony, S. Ehrlich and H. Krieg, *J. Chem. Phys.*, 2010, **132**, 154104.

S7 A. A. Peterson, F. Abild-Pedersen, F. Studt, J. Rossmeisl and J. K. Nørskov, *Energy Environ. Sci.*, 2010, **3**, 1311-1315.

S8 Z. Miao, Y. Zhang, N. Wang, P. Xu and X. Wang, *J. Colloid Interface Sci.*, 2022, **620**, 407-418.

S9 J. Zhao, Z. Miao, Y. Zhang, G. Wen, L. Liu, X. Wang, X. Cao and B. Wang, *J. Colloid Interface Sci.*, 2021, **593**, 231-243.

S10 J. Wu, X. Li, W. Shi, P. Ling, Y. Sun, X. Jiao, S. Gao, L. Liang, J. Xu, W. Yan, C. Wang and Y. Xie, *Angew. Chem., Int. Ed.*, 2018, **57**, 8719-8723.

S11 J. Di, C. Chen, C. Zhu, P. Song, M. Duan, J. Xiong, R. Long, M. Xu, L. Kang, S. Guo, S. Chen, H. Chen, Z. Chi, Y. Weng, H. Li, L. Song, M. Wu, Q. Yan, S. Li and Z. Liu, *Nano Energy*, 2021, **79**, 105429.

S12 D. Liu, D. Chen, N. Li, Q. Xu, H. Li, J. He and J. Lu, *Angew. Chem., Int. Ed.*, 2020, **59**, 4519-4524.

S13 C. Zhou, X. Shi, D. Li, Q. Song, Y. Zhou, D. Jiang and W. Shi, *J. Colloid Interface Sci.*, 2021, **599**, 245-254.

S14 J. Di, C. Chen, C. Zhu, R. Long, H. Chen, X. Cao, J. Xiong, Y. Weng, L. Song, S. Li, H. Li, Y. Xiong and Z. Liu, *Adv. Energy Mater.*, 2021, **11**, 2102389.

S15 K. Liu, X. Zhang, C. Zhang, G. Ren, Z. Zheng, Z. Lv and C. Fan, *RSC Adv.*, 2019, **9**, 14391-14399.

S16 X. Ren, M. Gao, Y. Zhang, Z. Zhang, X. Cao, B. Wang and X. Wang, *Appl. Catal. B: Environ.*, 2020, **274**, 119063.

S17 J. Di, C. Chen, C. Zhu, P. Song, J. Xiong, M. Ji, J. Zhou, Q. Fu, M. Xu, W. Hao, J. Xia, S. Li, H. Li and Z. Liu, *ACS Appl. Mater. Interfaces*, 2019, **11**, 30786-30792.

S18 M. Gao, J. Yang, T. Sun, Z. Zhang, D. Zhang, H. Huang, H. Lin, Y. Fang and X. Wang, *Appl. Catal. B: Environ.*, 2019, **243**, 734-740.

S19 Y. Feng, J. Xie, Z. Lu, A. Hao, J. Hu and Y. Cao, *J. Nanopart. Res.*, 2022, **24**, 27.

S20 D. Wu, L. Ye, H. Y. Yip and P. K. Wong, *Catal. Sci. Technol.*, 2017, **7**, 265.

S21 X. Jin, C. Lv, X. Zhou, H. Xie, S. Sun, Y. Liu, Q. Meng and G. Chen, *Nano Energy*, 2019, **64**, 103955.

S22 J. Zhu, Y. Li, X. Wang, J. Zhao, Y. Wu and F. Li, *ACS Sustain. Chem. Eng.*, 2019, **17**, 14953-14961.

S23 L. Ye, X. Jin, C. Liu, C. Ding, H. Xie, K. H. Chu and P. K. Wong, *Appl. Catal. B: Environ.*, 2016, **187**, 281-290.

S24 D. Wu, L. Ye, S. Yue, B. Wang, W. Wang, H. Y. Yip and P. K. Wong, *J. Phys. Chem. C*, 2016, **120**, 7715-7727.

S25 L. Wang, G. Liu, B. Wang, X. Chen, C. Wang, Z. Lin, J. Xia and H. Li, *Sol. RRL*, 2021, **5**, 2000480.